RAD Conference Proceedings, vol. 1, pp. 117-123, 2016
www.rad-proceedings.org

$BaCe_{0.85}Y_{0.15}O_{3-\Delta}$ BASED MATERIALS FOR SOLID OXIDE FUEL CELLS: ROOM-TEMPERATURE NEUTRON DIFFRACTION STUDY

K. Krezhov[1*], D. Vladikova[2], G. Raikova[2], T. Malakova[1], I. Genov[2], Tz. Nonova[1], E. Svab[3], M. Fabian[4]

[1]Institute for Nuclear Research and Nuclear Energy, Bulgarian Academy of Sciences, Sofia, Bulgaria
[2]Institute of Electrochemistry and Energy Systems, Bulgarian Academy of Sciences, Sofia, Bulgaria
[3]Wigner Center of Physics, RISSPO, Hungarian Academy of Sciences, Budapest, Hungary
[4]Center for Energy Research, Hungarian Academy of Sciences, Budapest, Hungary

Abstract. *The crystal structure of oxygen-deficient $BaCe_{0.85}Y_{0.15}O_{3-\delta}$ (BCY15) materials prepared by auto-combustion with following calcination at high temperature was determined from neutron and X-ray powder diffraction. The materials were used recently as cathode, anode and central membrane in a novel design of SOFC: dual membrane fuel cell (dmFC). The dmFC design exploits the good mixed (protonic and oxide ion) conductivity in $BaCe_{0.85}Y_{0.15}O_{2.825}$ at working temperatures of 600-700 °C. It allows the introduction of a separate compartment (central membrane) for water formation and evacuation. The central membrane has mixed ionic conductivity ensured by a composite material and porous microstructure. Profile refinements within the orthorhombic space group Pnma reproduced the neutron diffraction profiles of all the materials (dense, porous, powder) based on BCY15 conductivity presenting similar model crystal structures to protonic conductor $BaCe_{0.9}Y_{0.10}O_{2.95}$ and the parent undoped BaCeO3 perovskite.*

***Key words*:** *Perovskites, doped barium cerate, proton conductor, crystal structure, fuel cells*

DOI: 10.21175/RadProc.2016.28

1. INTRODUCTION

As the world-wide demand for energy is expected to continue to increase, the development of improved technologies for sustainable, environmentally-friendly and efficient production, storage and use of energy is one of the major challenges. Materials are essential component to improved performance in a number of leading energy technologies including energy storage in batteries and supercapacitors and energy conversion through solar cells, fuel cells, and thermoelectric devices. The pursuit for innovative energy technologies relies on both soft and hard matter materials. Neutrons are a vital analytical tool, as they afford deep insight into the structure and dynamics of matter. In particular, their high penetration depth allows studies on complex systems and fully assembled devices under in situ/operando conditions. Besides, the functionality of most energy related materials is intimately connected to the presence of light atoms as hydrogen, lithium or oxygen and the neutrons are ideally suited to elucidate the appropriate structures and dynamics.

In this study we report results from our neutron diffraction investigation on the powder, dense and porous materials based on the composition $BaCe_{0.85}Y_{0.15}O_{3-\delta}$ (BCY15) with potential use in a new design of solid oxide fuel cells as described below.

2. SOLID OXIDE FUEL CELLS. GENERAL DESCRIPTION

Solid oxide fuel cells (SOFCs) offer a promising green technology of direct conversion of chemical energy of fuel into electricity [1,2]. SOFC is a class of fuel cells characterized by the use of a solid oxide (ceramic) component as the electrolyte, Figure 1.

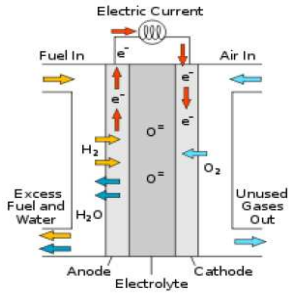

Figure 1. Sketch of a solid oxide fuel cell. The highly dense ceramic electrolyte is sandwiched between two porous electrodes, the anode and the cathode. Fuel is fed to the anode, where it undergoes an oxidation reaction, and releases electrons to the external circuit. Oxidant is fed to the cathode, accepts electrons from the external circuit, and undergoes a reduction reaction. The electron flow in the external circuit from the anode to the cathode produces electricity.

The anode/electrolyte/cathode sandwich forms a single cell, typically a few millimetres thick. The

* kiril.krezhov@gmail.com

generated voltage varies from 0.7 to 1.4 volt. Large number of these cells is connected together in series to make a battery called as fuel cell battery, fuel battery or "SOFC stack" [3]. The DC current produced by a fuel cell battery is later converted into AC current using an inverter. Electricity power ranging from 1 kW to 200 kW can be obtained for domestic or industrial use.

The ceramics used in SOFCs do not become electrically and ionically active until they reach high temperature so that the operating temperatures are ranging from 600 to 1,000 °C. Reduction of oxygen gas (O2) into oxygen ions (O^-) occurs on the cathode side. The O^- ions can diffuse through the solid oxide electrolyte to the anode where they can electrochemically oxidize the fuel. In all types of fuel cell, hydrogen is used as fuel and can be obtained from any source of hydrocarbon. In this reaction, a water byproduct is given off as well as two electrons. The produced electrons flow through an external circuit doing useful work and the cycle then repeats as those electrons enter the cathode material again.

Finding appropriate combinations of electrolyte and electrode materials that provide both rapid ion transport across the electrolyte and electrode-electrolyte interfaces and efficient electrocatalysis of the oxygen reduction and fuel oxidation reactions remains a significant materials challenge [1-4]. Fig. 2 illustrates the general complications to achieve highly efficient SOFCs.

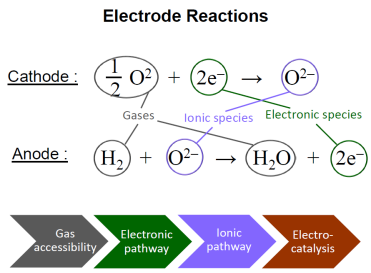

Figure 2. Main issues in the designs of SOFCs

2.1. $BaCe_{1-x}Y_xO_{3-\delta}$ in SOFCs

The advancement of highly efficient ion conduction materials is essential to the development of SOFC and other electrochemical devices such as batteries and hydrogen sensors. The quest is on solid oxide materials with high ionic conductivity while preserving structural stability at high temperatures.

Detailed characterization of the electric properties of many candidate oxide materials as a function of temperature and atmosphere has been reported. The oxygen-deficient ceramics of oxides with perovskite-like structure $A^{2+}B^{4+}O_3$, (A^{2+} = Pb or some alkaline earth ions such as Ba, Sr, etc.; B^{4+} = Ce, Ti, Nb, Zr, Mo, etc.) are recognized among the most efficient materials that can be used as electrolytes or electrodes (metal-ceramic electrode structures) in SOFCs [1,5,6]. In these ABO_3 oxides the B cation is partially substituted by a trivalent dopant (In^{3+},Y^{3+}, rare earth ions such as Gd^{3+}, Sm^{3+}, Nd^{3+}), introducing this way oxygen vacancy in the crystal lattice [7-9]. Oxygen-vacancy content is relevant to proton-conducting oxides in which protons are introduced via the dissolution of hydroxyl ions at vacant oxygen sites [10].

$BaCeO_3$ is well characterised as an electronic insulator and proton conductor. The phase adopts the orthorhombic perovskite structure in space group Pnma (No. 62), as shown by X-ray (synchrotron and laboratory sources) and neutron diffraction studies. The material is hygroscopic and adsorbs water dissociative with formation of hydroxyl groups. At elevated temperatures (>600 °C), hydrogen atoms in the structure become mobile. In this regard, the doped material of Barium cerate with Y-substitution at the perovskite B-site (Ce site) is well known for excellent conduction capabilities in the temperature range 400–800 °C as a result from the proton motion in the crystal lattice [6]. Doping with Y^{3+} is very effective making $BaCe_{1-x}Y_xO_{3-\delta}$ a feasible candidate for solid state proton electrolyte applications in fuel cells. The proton conductivity increases with the increasing of the dopant concentration up to x =0.2 (BCY20) for which a high total conductivity of $\approx 5{,}3.10^{-2}$ $(\Omega cm)^{-1}$ was reported in a hydrogen containing atmosphere [10,11].

For BCY20 rich structural phase transformations as a function of temperature and water uptake were found to occur by structure sensitive techniques [12-18]**.** The oxides $BaCe_{1-x}Y_xO_{3-\delta}$ with lower substitution rate ($x \leq 0.15$) feature seemingly a higher structural stability [13,14,16]. Nevertheless, the crystalline structures even at ambient temperature remain questioned because depending on synthesis and processing conditions subtle local tilting and distortion of the Ce/Y containing oxygen octahedra results in various structures of monoclinic, rhombohedral and orthorhombic symmetry [12,18].

2.2 Proton conduction in $BaCe_{1-x}Y_xO_{3-\delta}$

As mentioned already, the studied barium cerate based materials are extrinsic systems since the proton defects, which are the charge carriers, are introduced in the crystal structure by dissolution of water vapor**.** The proton transport kinetics in the crystal lattice of these materials is closely related to the oxygen vacancies created by the Y^{3+} substituent. These vacancies can be filled with the oxygen from adsorbed water molecule and the introduced protons are bound to the lattice oxygen. Thermal activation acts as the driving force for the protons to overcome an energy barrier of a few hundred eV and jump to another oxygen site and thus constituting proton mobility.

The conduction phenomena may be explained by an appropriate defect model (Kroger–Vink notation). Under humidified conditions, hydroxide species can be produced by the oxidation of water vapor as shown in Equation (1). Water vapor dissociates into a hydroxide ion, which fills an oxide-ion vacancy V_O^{**}, and a proton that forms a covalent bond with lattice oxygen O_O^x, i.e. two proton defects are created stoichiometrically [19]

$$H_2O_{(g)} + V_O^{**} + O_O^x \rightarrow 2OH_O^* \qquad (1)$$

In the presence of hydrogen, hydrogen can react with oxide ions in the lattice producing hydroxide groups and electrons as in Equation (2). It is believed that protons could migrate by hopping from the OH site to oxide ion site causing this material to exhibit proton conductivity [4,19]

$$\frac{1}{2}H_{2(g)}O_O^x \rightarrow OH_O^* + e^{'} \qquad (2)$$

In the presence of oxygen, the conduction phenomena should depend on the partial pressure of oxygen. At high oxygen partial pressure, the dissolution of oxygen into the crystal structure of these ceramics may occur as expressed in Equation (3) resulting in the creation of an oxide ion in the lattice and electron holes [7,8].

$$\frac{1}{2}O_{2(g)} + V_O^{**} \rightarrow O_O^x + 2h^* \qquad (3)$$

At low oxygen partial pressure, oxide ions may leave the lattice creating oxygen vacancies and electrons as expressed in Equation (4). Furthermore, at high temperatures oxide ions in the lattice may become excited and migrate to other oxygen vacancies nearby

$$O_O^x \rightarrow \frac{1}{2}O_{2(g)} + V_O^{**} + 2e' \qquad (4)$$

It deserves noting that although probable proton positions have been proposed it remains uncertain where exactly in the lattice the proton is located [16].

3. Dual membrane fuel cell. Monolithic design

The dual membrane fuel cell (dmFC) is a three compartment fuel cell based on a junction between a protonic ceramic fuel cell (PCFC) anode (anode/electrolyte) compartment and a SOFC cathode (electrolyte/cathode) compartment through a mixed (proton and oxide ion) conducting porous ceramic membrane. The original idea is the introduction of a separate compartment (central membrane, CM) for the water formation and evacuation. Protons created at the anode progress toward the CM where they meet the oxide ions created at the cathode and produce water. Water is then evacuated through the interconnecting porous media of the CM. Thus, the dmFC operates with three independent chambers for hydrogen, oxygen, and water and offers the possibility for optimization of each chamber. Fig. 3 shows the components at an early stage of use of BCY15 material [20,21].

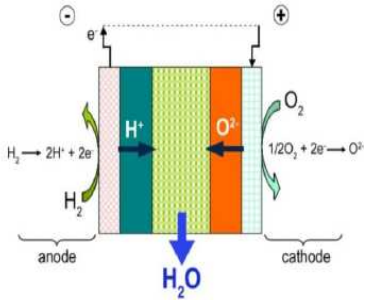

Figure 3. Dual Membrane Fuel Cell (dmFC) ("classical" design): anode: Ni/BCY15; anode electrolyte: BCY15 ($BaCe_{0.85}Y_{0.15}O_{2.925}$); composite central membrane: BCY15 + YDC15 ; cathode electrolyte: YDC15 ($Ce_{0.85}Y_{0.15}O_{1.925}$) ; cathode: LSCF ($La_{0.6}Sr_{0.4}CoFeO_{3-\delta}$)

The concept has important advantages: the fuel and the oxidizer are not diluted; water does not inhibit the catalytic activity of the electrodes [21,22].

Fig.4 illustrates the novel dual membrane-based configuration, named "monolithic" [23,24]. The design (Left panel) exploits the good mixed (protonic and oxide ion) conductivity in BCY15 (Right panel) at operating temperatures revealed by a specific electrochemical characterization performed by impedance measurements of a symmetrical half-cell Pt/BCY15/Pt in dry and wet hydrogen and oxygen [24]. The results show that at working temperatures 600-700°C the oxygen and hydrogen conductivities are similar and are sufficiently high for good performance which is competitive with data reported for conventional electrolytes. Thus in flow of oxygen (O2) BCY15 is oxide ion conductor, in flow of hydrogen (H2) it is proton conducting. In the central membrane it is mixed ion conducting.

This "single material" concept has better performance as fuel cell, but also as electrolyser, because the material has a natural property to split water. The challenge is to develop the monolithic design as a device which works in reversible mode – as a fuel cell and as an electrolyser. While the utmost interest is the macroscopic motion of hydrogen atoms in applied electric field better understanding of structure-property relationships is essential to reveal underlying mechanism.

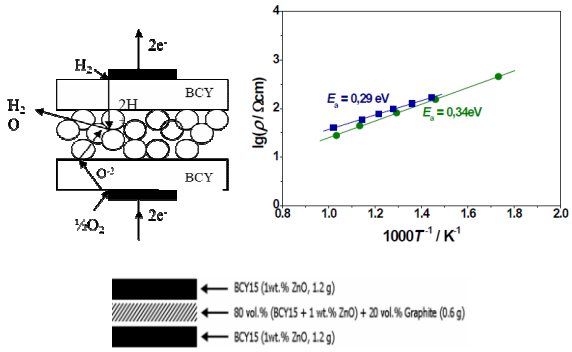

Figure 4. Monolithic dmFC [23]. Left: The 3-layered monolithic assembly built from BCY15 material works as oxide ion conductor in the oxygen space, as proton conductor in the hydrogen area and as mixed conductor in the central membrane; Right: Arrhenius plots of BCY15 in dry air (●) and wet hydrogen (■).

4. Experimental Section

BCY15 was prepared by auto-combustion technique starting from metal nitrates and using urea as reducing agent. Calcinations of the precursor at 1100-1150°C in inert atmosphere for complete CO_2 elimination ensured the production of single phase powder with desired chemical composition $BaCe_{0.85}Y_{0.15}O_{3-\delta}$ determined by ion coupled plasma analysis with dominating particle size of about 200 nm and minor degree of agglomeration. The BCY15 electrolyte support pellets (diameter/thickness = 20-25/1-1,3 mm) were prepared by cold pressing and sintering at a temperature of 1450°C. Initial characterization by X-ray diffraction, SEM and EDX shows BCY15 material with grain size 35-50 μm and density approximately 95% relatively to the theoretical density. Porous material was obtained by mixing thoroughly the powder BCY15 with graphite powder and firing the mixture at 1450°C.

The structural characterization of polycrystalline BCY15 was carried out using a Bruker D8 Advanced diffractometer (40 kV, 30 mA) in Bragg-Brentano reflection geometry. The Topas-4.2 software was used to analyse the XRD patterns collected with Cu Kα

radiation (λ= 1.5418 Å) and LynxEye PSD detector at 20 °C within the angular range from 10° to 120° 2θ with a constant step 0.20° 2θ and 175 sec/step counting time. To improve the statistics, sample rotating speed of 30 rpm was used. Phase identification was made with the Diffracplus EVA software using the International Centre for Diffraction Data (ICDD) PDF-4 database.

Neutron powder diffraction (NPD) studies were conducted by the time of flight method (TOF) and the method of constant wavelength. Correspondingly, two instrument were used: the spectrometer DN-12 [25] of JINR, Dubna at the reactor IBR-2M, which is a spectral source of neutron pulses with a frequency of 5 Hz and the high intensity instrument PSD [26] of the Budapest Neutron Centre at the reactor VVR-M, which is a continuous spectral neutron source with steady Maxwelian distribution of neutron wavelengths.

On the diffractometer PSD the NPD patterns were collected for wavelength λ = 1.069 Å, in scattering angle (2θ) range 3.60-114.0° at an angular step size of 0.10°. The samples were loaded into 50 mm long cylindrical thin-walled vanadium containers (dia. 6 mm). For the TOF spectrometer the samples were packed in 5 mm long cylindrical holders (dia. 3.5 mm) of thin aluminium foil. Diffraction patterns were collected for 4 h at scattering angle 2θ=90°, where the spectrometer resolution at λ = 2 Å is Δd/d = 0.012.

The XRD and ND data were analysed using the FULLPROF suite [27] by applying profile matching mode followed by full profile Rietveld refinement of the structural model. In neutron refinements a Thompson-Cox-Hastings pseudo-Voigt function was chosen to generate the line shape of the diffraction peaks and a fifth-degree polynomial function was applied for the fitting of the background. The tabulated coherent scattering lengths b_{coh} were used: 5.07, 4.84, 7.75 and 5.803 fm for Ba, Ce, Y and O, respectively. Bond valence analysis of the structures was made as well.

5. Results and discussion

The indexation of neutron powder diffraction (NPD) profiles measured with diffractometer PSD and DN-12 spectrometer, shown in Fig. 5 and Fig. 6 correspondingly, did not reveal any indications of difference in the crystallographic symmetry of individual samples. The NPD patterns were collected on representative powder samples of the three types of BCY15 based material at 295 K and ambient pressure.

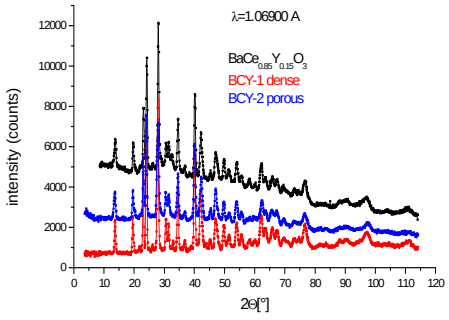

Figure 5. NPD patterns (λ = 1.0690 Å) of $BaCe_{0.85}Y_{0.15}O_{3-\delta}$ based materials at 295 K. The sample denoted as powder was kept for three days in moist air. The patterns are vertically shifted to improve visibility.

The multi-pattern mode of the FullProf program for simultaneous treatment of neutron and x-ray data sets was used to refine the structure and to determine the lattice parameters, atomic positions and thermal factors. We considered the undoped $BaCeO_3$ crystal structure as the starting structural model, with orthorhombic symmetry and space group Pnma (No.62), Z = 4 (formula units/cell); all the Bragg peaks of the diagram could be thus indexed. Barium and apical (out from (*ac*) plane) oxygen atoms (O_{ap}) occupy Wyckoff position 4*c* (x,1/4,z), Ce is in position 4*b* (1/2,0,0), and equatorial oxygen atoms (O_{eq}) in the (*ac)* plane occupy general position 8*d* (*x,y,z*). Yttrium atoms were introduced at random at 4b positions together with Ce, and the complementary occupancy factors were refined, constrained to a full occupancy. In the final refinement, the Ce/Y occupancy factors were unconstrained, indicating a slight deviation from the nominal 0.85:0.15 stoichiometry. In summary, profile refinements within the orthorhombic space group *Pnma* reproduced the RT-patterns of all samples reasonably well.

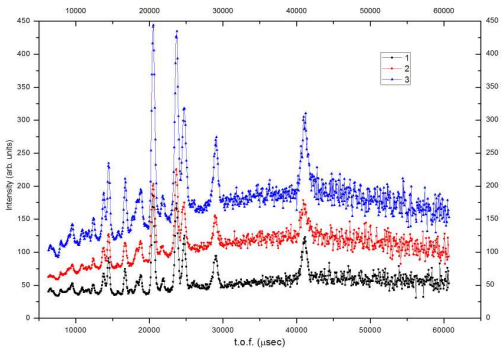

Figure 6. Time of flight patterns for representative samples of $BaCe_{0.85}Y_{0.15}O_{3-\delta}$ based samples at 295 K: 1 (dense), 2 (porous), 3 (powder). The patterns are vertically shifted to improve visibility.

Refinements in rhombohedral space group R-3c and monoclinic symmetry space group I2/m were also tested as well as a mixture of two perovskite-type phases of R-3c and I2/m symmetry was checked as recommended for this composition [16,17] but the agreement factors were not satisfactory.

Figure 7 presents the X-ray experimental data, the final full profile refinement and the difference between them for a powder material $BaCe_{0.85}Y_{0.15}O_{2.925}$ at 295 K. The material measured was annealed in hydrogen-free atmosphere and kept stored under dry atmosphere.

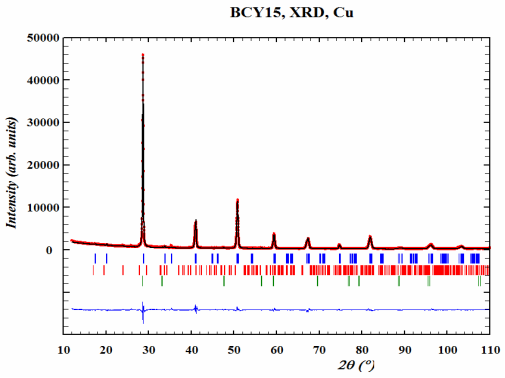

Figure 7. Room temperature Rietveld refined X-ray diffraction pattern of a powder sample with nominal composition $BaCe_{0.85}Y_{0.15}O_{2.925}$.The rows of tick marks give the positions of the allowed in Pnma space group Bragg reflections for the main phase of BCY15 (upper) and the minority phases of $BaCo_3$ (middle) and CeO_2 (lower). The difference curve between the observed and calculated intensities in the full profile analysis is presented at the bottom.

Traces of impurities, identified as CeO2 and BaCo3, were detected by the XRD diffraction analysis. Although the as-prepared substance was kept in a vessel under dry air, the revealed presence of minor phases of the order of 1,2 wt% each one supports the claims that one major disadvantage of barium cerate based materials is their poor chemical stability in long term. Generally, in the presence of carbon dioxide barium carbonate and cerium(IV) oxides are produced in the reaction [1, 28]:

$$BaCeO_3 + CO_2 \rightarrow BaCO_3 + CeO_2 \qquad (5)$$

Fig. 8 shows on the example of a powdered "dense" material the agreement between the observed and calculated NPD curves from the final Rietveld fit. The quantity of impurity phases turned out of being below the sensitivity at the given NPD experimental conditions. The final positional and isotropic thermal parameters obtained are listed in Table l, in which we include also the agreement factors describing the quality of the Rietveld refinement. The small deviations from the values published in [29] are due to the attempt to refine the parameter δ.

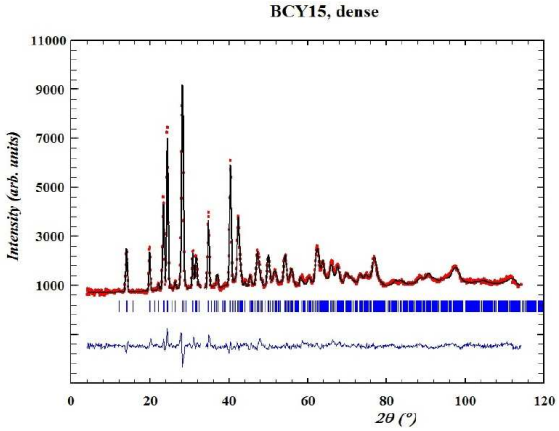

Figure 8. Observed (crosses), calculated (full line), and difference (at the bottom) NPD profiles for powdered dense BCY15 based material at 295 K refined in the orthorhombic Pnma space group. The vertical markers correspond to the allowed Bragg reflections.

Table 1. Fractional atomic coordinates and isotropic thermal parameters of $BaCe_{0.85}Y_{0.15}O_{3-\delta}$ (δ = 0.06±0.02) as refined in S.G. *Pnma (Z=4)*. Unit cell parameters* (Å): *a*= 6.2092(9), *b*= 8.8272 (6), *c*= 6.2053(8), volume (Å³) = 340.11(25). Agreement factors (%): R_{wp} =5.90, R_B = 3.64, χ^2= 1.84. Estimated standard deviations are in parenthesis.

	x	y	z	B, Å²
Ba	0.0096(5)	0.25	-0.0019(7)	1.24(5)
Ce/Y	0	0	0.5	0.52(6)
O_{ap}	0.4593(5)	0.25	0.1013(7)	0.87(6)
O_{eq}	0.2457(4)	0.0494(7)	0.7465(7)	0.87(6)

*The data evidence a low spontaneous orthorhombic stress s=-3.1.10^{-4} defined by the expression $s=2(c-a)/(a+c)$.

The unit cell parameters of $BaCe_{0.85}Y_{0.15}O_{3-\delta}$ are close to the values of $BaCeO_3$ and $BaCe_{0.9}Y_{0.1}O_{2.95}$ given in the references included in the ICDD PDF-4 database. The relationships between the parameters is a > c and a > b/√2 > c, which is typical for O-type perovskites, where the tilting of the octahedra is the main reason for the deviation from the ideal perovskite structure. The ideal perovskite structure is cubic (Pm–3m) in which the B-cations are surrounded by six anions arranged in corner- sharing octahedral geometry. This arrangement forms cubooctahedral cavity in which the A-cation is placed. In general, the distortion of the ideal perovskite structure is manifested by (1) tilting of the BO_6 octahedra; (2) deformation of the BO_6 octahedra and (3) displacement of the B-cation from the center of the octahedra [25]. In the investigated materials based on Y doped barium cerate the tilting of the octahedra decreases the ideal cubic symmetry to the orthorhombic O-type one.

Fig.9 illustrates the attempt for refinement of the structure of a protonated sample. In this experiment the sample studied was stored at ambient temperature in a closed vessel in air of controlled humidity of 90%. As already mentioned, hydroxide species can be produced by the oxidation of water vapor; water vapor dissociates into OH^-, which occupies one oxygen ion vacancy and the remaining H^+ forms with a lattice O^{2-} ion another OH^- as shown in Equation (1).

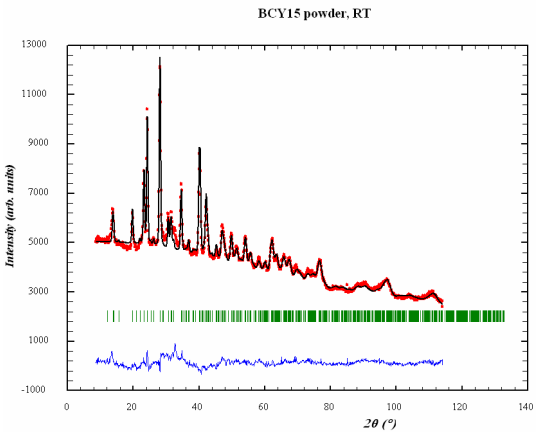

Figure 9. Observed (crosses), calculated (full line), and difference (at the bottom) NPD profiles of BCY15 protonated powder at 295 K refined in the *Pnma* space group. The row of tick marks gives the positions of the allowed Bragg reflections.

The extensive incoherent scattering of hydrogen from the hydroxyl groups is reflected by the steadily rising contribution to the background with decreasing to zero scattering angles. The fit is not of the required quality to allow for drawing up unambiguous conclusions for the structural details, in particular for which oxygen of corresponding octahedron in the structure is "attached" the proton. By simultaneous treatment of multiple powder diffraction datasets obtained by present constant wavelength X-ray and neutron diffraction experiments the powder overlap problem is only partially resolved in a Rietveld refinement.

The effect of the multi pattern Rietveld analysis is effectively to deconvolute the overlapping reflections by differing shifts in their relative positions. The medium resolution neutron powder data however have restricted the solution of the peak overlap problem in the structure models with protons.

In general, the studies focused on locating the proton within the crystalline structure are not rich in details and profound enough to obtain a good understanding of the effects of nonstoichiometry on the perovskite structure. Further neutron scattering experiments including neutron diffraction and quasi-elastic neutron scattering (QENS) studies should rely on samples with better known proton content.

CONCLUSIONS

$BaCe_{0.85}Y_{0.15}O_{3-\delta}$ (BCY15) oxygen deficient material prepared by auto-combustion with following calcination at high temperature was found to crystallize in orthorhombic Pnma space group and similarly to parent BaCeO3 stoichiometric perovskite and doped compound $BaCe_{0.9}Y_{0.1}O_{2.95}$ the crystalline structure belongs to the O-type distorted perovskites. This study may suggest that the oxygen-vacancy related defects in the BCY15structure are very sensitive to the processing conditions. The results of the present analysis can be useful in structural studies of $BaCeO_3$-based solid solutions and related materials.

Acknowledgement: *This research is partially funded from the Bulgarian National Fund for Science under grant E02/3 2014. The authors would like to thank Prof. Dr. D. Kovacheva from IGIC-BAS for valuable discussions and practical support of the XRD experiment.*

REFERENCES

1. T.A. Adams , J. Nease, D. Tucker and P.I. Barton, "Energy Conversion with Solid Oxide Fuel Cell Systems: A Review of Concepts and Outlooks for the Short- and Long-Term," *Ind. Eng. Chem. Res.*, vol. 52, no. 9, pp. 3089–3111, 2013
2. L. Malavasi, C.A.J. Fisher and M.S. Islam, "Oxide-Ion and Proton Conducting Electrolyte Materials for Clean Energy Applications: Structural and Mechanistic Features," *Chem. Soc. Rev.*, vol. 39, no. 11, pp. 4370-4387, 2010
3. *High Temperature Solid Oxide Fuel Cells: Fundamentals, Design and Applications*, S.C. Singhal and K. Kendall, Eds., Amsterdam, Netherlands: Elsevier, 2003
4. H. Iwahara, Y. Asakura, K. Katahira and M. Tanaka, "Prospect of Hydrogen Technology Using Proton-Conducting Ceramics," *Sol. St. Ionics*, vol. 168, no. 3-4, pp. 299-310, Mar. 2004
5. A. Bassano et al., "Synthesis of Y-doped $BaCeO_3$ Nanopowders by a Modified Solid-State Process and Conductivity of Dense Fine-Grained Ceramics," *Sol. St. Ionics*, vol. 180, no. 2-3, pp. 168-174, Mar. 2009
6. H. Iwahara, H. Uchida, K. Ono and K. Ogaki, "Proton Conduction in Sintered Oxides Based on $BaCeO_3$", *J. Electrochem. Soc.*, vol. 135, no. 2, pp. 529-533, 1988
7. I. Kosacki and H.L. Tuller, "Mixed Csonductivity in $SrCe_{0.95}Yb_{0.05}O_3$ Protonic Conductors," *Sol. St. Ionics*, vol. 80, no. 3-4, pp. 223-229, Sep. 1995
8. H. Iwahara, T. Yajima, T. Hibino and H. Ushida, "Performance of Solid Oxide Fuel Cell Using Proton and Oxide Ion Mixed Conductors Based on $BaCe_{1-x}Sm_xO_{3-\alpha}$," *J. Electrochem. Soc.*, vol. 140, no. 6, pp. 1687-1691, 1993
9. W. Suksamai and I.S. Metcalfe, "Measurement of Proton and Oxide Ion Fluxes in a Working Y-Doped $BaCeO_3$ SOFC," *Sol. St., Ionics*, vol. 178, no. 7-10, pp. 627-634, Apr. 2007
10. H. Iwahara, T. Yajima and H. Uchida, "Effect of Ionic Radii of Dopants on Mixed Ionic Conduction (H^++O^{2-}) in $BaCeO_3$-Based Electrolytes," *Sol. St. Ionics*, vol. 70-71, pt. 1, pp. 267-271, May-June 1994
11. G. Raikova et al., "Impedance Investigation of $BaCe_{0.8}Y_{0.2}O_{3-\delta}$ Properties for Hydrogen Conductor in Fuel Cells", *Bulg. Chem. Comm.*, vol. 44, no. 4, pp. 389-394, 2012
12. L. Malavasi, C. Ritter and G. Chiodelli, "Correlation between Thermal Properties, Electrical Conductivity, and Crystal Structure in the $BaCe_{0.8}Y_{0.2}O_{2.9}$ Proton Conductor," *Chem. Mater.*, vol. 20, no. 6, pp. 2343–2351, 2008
13. K.S. Knight, "Structural Phase Transitions, Oxygen Vacancy Ordering and Protonation in Doped $BaCeO_3$: Results from Time-Of-Flight Neutron Powder Diffraction Investigations," *Sol. St. Ionics*, vol. 145, no. 1-4, pp. 275–294, Dec. 2001
14. K.S. Knight, "Powder Neutron Diffraction Studies of $BaCe_{0.9}Y_{0.1}O_{2.95}$ and $BaCeO_3$ at 4.2 K: a Possible Structural Site for the Proton," *Sol. St. Ionics*, vol. 127, no. 1-2, pp. 43-48, Jan. 2000
15. K. Takeuchi, C.-K. Loong, J.W. Richardson Jr., J. Guan, S.E. Dorris and U. Balachandran, "The Crystal Structures and Phase Transitions in Y-Doped $BaCeO_3$: Their Dependence on Y Concentration and Hydrogen Doping", *Sol. St. Ionics*, vol. 138, no. 1-2, pp. 63–77, Dec. 2000
16. K. S. Knight, "Oxygen Vacancy Ordering in Neodymium-Doped Barium Cerate," *Sol. St. Comm.*, vol. 112, no. 2, pp. 73-78, Sep. 1999
17. C.K. Loong, M. Ozawa, K. Takeuchi, U. Koichi and N. Koura, "Neutron Studies of Rare Earth-Modified Zirconia Catalyst and Yttrium-Doped Barium Cerate Proton-Conducting Ceramic Membranes," *J. Alloys Compd.*, vol. 408-412, pp. 1065–1070, Feb. 2006
18. D. Han, M. Majima and T. Uda, "Structure Analysis of $BaCe_{0.8}Y_{0.2}O_{3-\delta}$ in Dry and Wet Atmospheres by High-Temperature X-Ray Diffraction Measurement," *J. Sol. St. Chem.*, vol. 205, pp. 122–128, Sep. 2013
19. T. Scherban and A.S. Nowick, "Bulk Protonic Conduction in Yb-Doped $SrCeO_3$," *J. Sol. St. Ionics*, vol. 35, no. 1-2, pp. 189-194, July-Aug. 1989
20. A.S. Thorel et al., "IDEAL-Cell, a High Temperature Innovative Dual mEmbrAne Fuel-Cell," *ECS Transact.*, vol. 25, no.2, pp.753-762, 2009
21. A. Thorel, "Cellule de pile a combustible haute temperature a conduction mixte anionique et protonique", Patent N° 0550696000, Mar. 17, 2005. (Fuel Cell with Mixed High-Temperature Anion and Proton Conductivity)
22. D. Vladikova et al., "Impedance Spectroscopy Studies of Dual Membrane Fuel Cell," *Electrochem. Acta*, vol. 56, no. 23, pp. 7955-7962, Sep. 2011
23. A. Thorel, D. Vladikova, Z. Stoynov, A. Chesnaud, M. Viviani and S. Presto, "Fuel Cell with Monolithic

Electrolytes Membrane Assembly," Patent no. 10 20120156573 (US 20120156573 A1), June 17, 2012
24. Z.B. Stoynov, D.E. Vladikova and E.A. Mladenova, "Gigantic Enhancement of the Dielectric Permittivity in Wet Yttrium-Doped Barium Cerate," *J. Sol. St. Electrochem.*, vol. 17, no. 2, pp. 555-560, Feb. 2013
25. Web site of Budapest Neutron Centre. Retrieved from: http://www.bnc.hu
26. Web site of IBR2 User Club. Retrieved from: http://ibr-2.jinr.ru
27. *FullPrf Suit, a set of crystallographic programs.* Retrieved from: https://www.ill.eu/sites/fullprof/
28. K. Przybylski, J. Prazuch, T. Brylewski, R. Amendola, S. Presto and M. Viviani, "Chemical Stability Study of Barium Cerate - Based Ionic Conducting Materials," in *Proceed. Int. Worksh. Advanc, Innov. SOFCs*, Katarino, Bulgaria, 2011, pp. 62 -71
29. K.A. Krezhov et al., "Structure Study of $BaCe_{0.85}Y_{0.15}O_{3-\Delta}$ (BCY_{15}) as Solid Oxide Fuel Cell Materal," in *Proceed. AIP Conf.*, Istanbul, Turkey, Aug. 2015